Journal of the European Ceramic Society **18** (1998) 1479–1492

PII: S0955-2219(98)00023-5
0955-2219/98/$—see front matter

J-Phase Solid Solution Series in the Dy–Si–Al–O–N System

K. Liddell,[a] D. P. Thompson,[a]* P. L. Wang,[b] W. Y. Sun,[b] L. Gao[b] and D. S. Yan[b]

[a]Materials Division, Department of Mechanical, Materials and Manufacturing Engineering, University of Newcastle, Newcastle upon Tyne, NE1 7RU, UK

[b]State Key Lab of High Performance Ceramics and Superfine Microstructure, Shanghai Institute of Ceramics, Chinese Academy of Sciences, Shanghai 200050, China

(Received 14 November 1997; revised version received 26 January 1998; accepted 2 February 1998)

Abstract

Detailed studies on J-phase compositions of the type $Dy_4Si_{2-x}Al_xO_{7+x}N_{2-x}$ *have demonstrated the existence of five different types of structure, all based on the monoclinic cuspidine arrangement characteristic of the end-members* $Dy_4Si_2O_7N_2$ *and* $Dy_4Al_2O_9$. *Series 1 and 3 extend into the system from the end-members, in the ranges* $0 \leq x \leq 0{\cdot}4$ *and* $1{\cdot}6 \leq x \leq 2{\cdot}0$, *respectively. Series 2 is characterised by a lower value of the b lattice parameter and occurs in the range* $0{\cdot}5 \leq x \leq 1{\cdot}5$, *while Series 4 is observed in the range* $0{\cdot}8 \leq x \leq 1{\cdot}1$ *alongside Series 2. Series 5 occurs in the range* $1{\cdot}4 \leq x \leq 1{\cdot}5$, *at which point X-ray patterns are much simpler, indexing on an orthorhombic unit cell with a halved c-axis repeat. These observations are consistent with structural differences observed in naturally-occurring cuspidine minerals, and also with recent observations on phase transformations in mixed rare earth* $Ln_4Al_2O_9$ *compounds.* © *1998 Elsevier Science Limited. All rights reserved*

1 Introduction

YAM, $Y_4Al_2O_9$, is the most yttrium rich of the three yttrium aluminates, and is also the most crystallographically complex. It has a structure based on cuspidine, $Ca_4Si_2O_7F_2$, and this[1] and the isostructural europium aluminate, $Eu_4Al_2O_9$[2], (Fig. 1) provided the original crystal structure determinations for structures of this type. When silicon nitride is densified with yttrium oxide, one of the grain boundary phases observed is $Y_4Si_2O_7N_2$[3] which Morgan[4] showed was isostructural with $Y_4Al_2O_9$. This phase is commonly referred to as J-phase[5] or N-YAM, even though a more logical designation might be N-cuspidine,[6] consistent with the mineral nomenclature used for other Y–Si–O–N phases.[5] A recent powder crystal structure refinement by McKenzie *et al.*[7] has confirmed that $Y_4Si_2O_7N_2$ does have the cuspidine structure. Original reports of complete solid solution between $Y_4Al_2O_9$ and $Y_4Si_2O_7N_2$[8] were subsequently doubted,[9] even though intermediate compositions were clearly cuspidine-like. During the last ten years, various patents have been taken out on silicon nitride materials containing $Y_4Si_2O_7N_2$ as the grain-boundary phase because of the increase in strength observed when this phase is crystallised from the grain-boundary glass and because of the good oxidation resistance of the product.[10–13]

Investigations have also been extended into rare earth systems. Thus rare earth aluminates of the type $Ln_4Al_2O_9$ are isostructural with YAM.[2,14–19] They are least stable for low-Z analogues (neither La nor Ce form a stable $Ln_4Al_2O_9$ phase) and the stability increases with increasing rare earth atomic number.[15] Related oxynitrides of formula $Ln_4Si_2O_7N_2$ have been reported for all lanthanide elements[6,20–22] and there is a uniform variation in unit cell dimensions as a function of rare earth atomic number for both the $Ln_4Al_2O_9$ and $Ln_4Si_2O_7N_2$ series (Figs 2 and 3). Even though the pseudo solid solution between $Y_4Si_2O_7N_2$ and $Y_4Al_2O_9$ has been explored in some detail,[9] similar studies have not been carried out in equivalent rare earth systems. The present paper describes a detailed study of cuspidine-type phases occurring along the $Dy_4Si_2O_7N_2$–$Dy_4Al_2O_9$ line of compositions.

A characteristic feature of early crystallographic work on oxynitride J-phases was the confusion

*To whom correspondence should be addressed.

over the choice of unit cell. Brandle and Steinfink[2] used the cuspidine cell with $a \approx 7$ Å and $c \geq 11$ Å and space group $P2_1/c$ to describe $Eu_4Al_2O_9$. Subsequent researchers have tended to exchange the a and c parameters, in which case the space group is $P2_1/a$. The main source of confusion is that for all these structures (described using the $a \approx 11$ Å, $c \approx 7$ Å unit cell), $a\cos(180\text{-}\beta)$ is very nearly equal to $c/2$, as a result of which there is a pseudo-orthorhombic cell with $a_o \approx 2a_m \sin\beta$ and unchanged b and c dimensions (Fig. 4) and an alternative monoclinic cell with almost identical unit cell dimensions to the conventional cell, but indexing in space group $P2_1/n$. Moreover, X-ray reflections with odd l (referred to c as the short axis) are very weak, indicating a pseudo-halving of the structure in the c direction. As a result, the X-ray patterns for $Y_4Al_2O_9$ and $Y_4Si_2O_7N_2$ can each be indexed using two possible sets of monoclinic unit cell parameters as follows:

$Y_4Al_2O_9$	(1)	$a = 11{\cdot}1224$, $b = 10{\cdot}4663$, $c = 7{\cdot}3743$ Å; $\beta = 108{\cdot}563°$
	(2)	$a = 11{\cdot}2190$, $b = 10{\cdot}4663$, $c = 7{\cdot}3743$ Å; $\beta = 109{\cdot}980°$
$Y_4Si_2O_7N_2$	(1)	$a = 10{\cdot}7334$, $b = 10{\cdot}4621$, $c = 7{\cdot}5627$ Å; $\beta = 110{\cdot}081°$
	(2)	$a = 10{\cdot}8010$, $b = 10{\cdot}4621$, $c = 7{\cdot}5627$ Å; $\beta = 111{\cdot}039°$

The strong diffraction lines index in space group $P2_1/a$ or $P2_1/n$ for both unit cells, and this does not allow unique differentiation between the two possibilities. Only by examining the weak, odd l lines on the photographs closely can the correct space group be established. Table 1 shows the

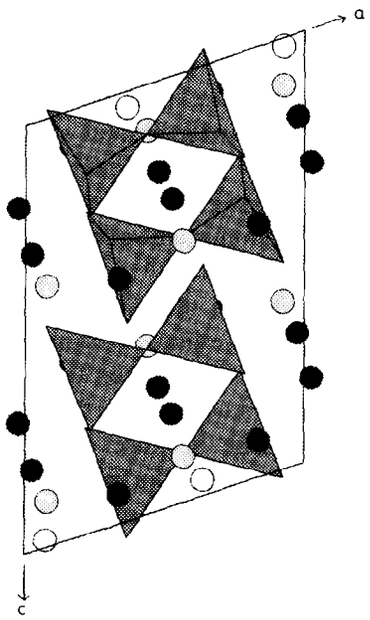

Fig. 1. [010] projection of $Eu_4Al_2O_9$ after Ref. 2 (•, Eu; o, O; △, AlO_4 tetrahedra).

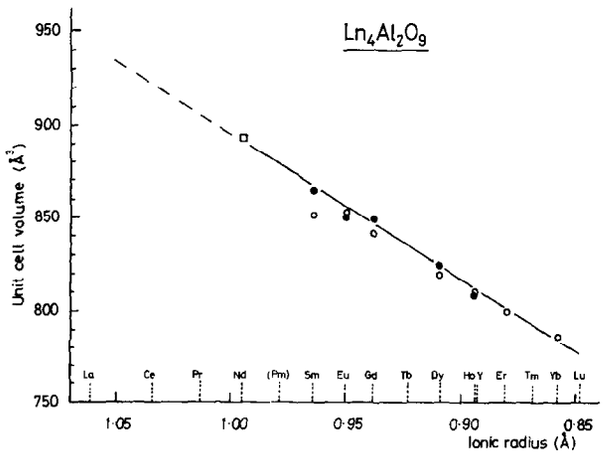

Fig. 2. Range of unit cell dimensions for rare earth $Ln_4Al_2O_9$ phases (□, after Ref. 14; •, after Ref. 2; o, after Refs 15–19).

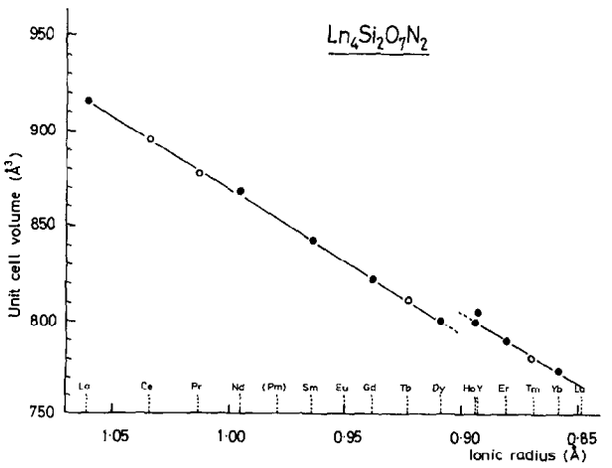

Fig. 3. Range of unit cell dimensions for rare earth $Ln_4Si_2O_7N_2$ phases (•, after Ref. 6; o, after Ref. 21).

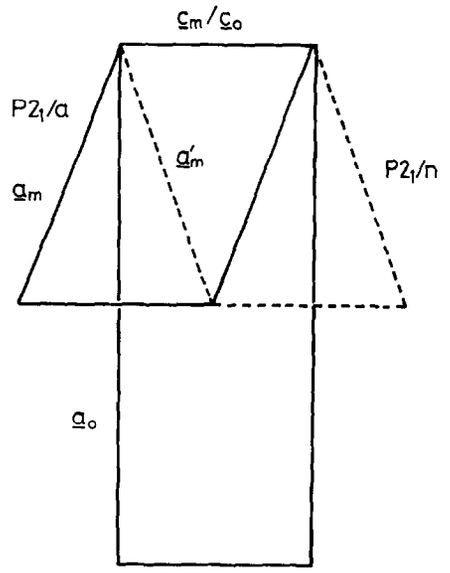

Fig. 4. Relationship between the conventional $P2_1/a$ cuspidine cell, the equivalent $P2_1/n$ cell and the larger pseudo-orthorhombic cell

key reflections for this purpose, and it is clear that $Y_4Al_2O_9$, cell (1), with the smaller a and β angle, must be used with space group $P2_1/a$ and cell (2) with $P2_1/n$; likewise for $Y_4Si_2O_7N_2$, the same conclusion holds. Since $P2_1/n$ is not a conventional monoclinic space group, it is recommended that the $P2_1/a$ space group cell should be used with the associated type (1) dimensions. This conclusion is consistent with previous data for $Y_4Al_2O_9$ and for the $Eu_4Al_2O_9$ structure determination.[2] but other data reported in the literature for $(Ln,Y)_4Si_2O_7N_2$ phases have been indexed in either orientation. It is recommended that future indexings of J-phases should be reported in space group $P2_1/a$. Tables 2 and 3 show the complete X-ray patterns for $Y_4Al_2O_9$ and $Y_4Si_2O_7N_2$, respectively, indexed in this way. This convention has been applied to all the Dy J-phases reported in the present paper.

Table 1a. X-ray reflections of odd l used for the confirmation of space group and unit cell for Y_4Al_2O

d_{obs}	d_{calc}	*hkl (1)*	*hkl (2)*	*Conclusion*
6·9918	6·9906	001	$\bar{1}01$	(1)≡$P2_1/a$ (2)≡$P2_1/n$
	6·9304	$\bar{1}01$	001	Poor agreement
5·0488	5·0529	$\bar{2}01$	101	(1)≡$P2_1/a$ (2)≡$P2_1/n$
	5·1234	101	$\bar{2}01$	Poor agreement
3·6863	3·6868	$\bar{1}02$	$\bar{1}02$	Not permitted either
	3·6831	201	$\bar{3}01$	(1)≡$P2_1/a$ (2)≡$P2_1/n$
	3·6610	121	$\bar{2}21$	Poor agreement
2.4388	2·4479	$\bar{1}41$	041	Permitted both
	2·4452	$\bar{1}03$	$\bar{2}03$	(1)≡$P2_1/a$ (2)≡$P2_1/n$
	2·4374	$\bar{2}03$	$\bar{1}03$	(1)≡$P2_1/a$ (2)≡$P2_1/n$
1·9199	1·19261	$\bar{3}33$	033	Poor agreement
	1·9125	341	$\bar{4}41$	(1)≡$P2_1/a$ (2)≡$P2_1/n$
	1·9125	341	$\bar{4}41$	Poor agreement
1·6841	1·6855	313	$\bar{6}13$	Permitted both
	1·6843	$\bar{6}03$	303	(1)≡$P2_1/a$ (2)≡$P2_1/n$
	1·6804	233	$\bar{5}33$	Poor agreement

Table 1b. X-ray reflections of odd l used for the confirmation of space group and unit cell for $Y_4Si_2O_7N_2$

d_{obs}	d_{calc}	*hkl (1)*	*hkl (2)*	*Conclusion*
7·1139	7·1029	001	$\bar{1}01$	(1)≡$P2_1/a$ (2)≡P21/n
	7·0586	$\bar{1}01$	001	Poor agreement
5·0460	5·0475	101	$\bar{2}01$	200 overlap
	5·0404	200	200	hk0 reflection dominant
5·0037	4·9999	$\bar{2}01$	101	(1)≡$P2_1/a$ (2)≡$P2_1/n$
2·4998	2·5043	$\bar{1}03$	$\bar{2}03$	Poor agreement
	2·5000	$\bar{4}02$	202	l = 2n dominant
	2·4984	$\bar{2}03$	$\bar{1}03$	h02 overlap
1·9055	1·9059	203	$\bar{5}03$	(1)≡$P2_1/a$ (2)≡$P2_1/n$
1·6659	1·6666	$\bar{6}03$	303	(1)≡$P2_1/a$ (2)≡$P2_1/n$
	1·6625	441	$\bar{5}41$	Poor agreement
	1·6621	$\bar{2}34$	$\bar{2}34$	Poor agreement

2 Experimental

Compositions were prepared in the compositional range $Dy_4Si_{2-x}Al_xO_{7+x}N_{2-x}$ using starting powders Dy_2O_3 (Aldrich Chemicals 99·9%), Si_3N_4 (Starck LC10), Al_2O_3 (Alcoa A16) and SiO_2 (BDH precipitated); compensation was made for 4 w/o surface SiO_2 in the Si_3N_4. Powders were mixed by hand in iso-propanol and pressed uniaxially and isostatically into 5 g pellets; each was embedded in a graphite crucible packed with a mixture of 50:50 BN:Si_3N_4 by weight. All samples were fired in a graphite element furnace for one hour at 1700°C or 1750°C; some of the latter were believed to have reached a temperature of >1950°C for ≈1–2 min caused by a temporary fault in the heating controller. X-ray diffraction analysis was carried out, with KCl as internal standard, using a Hägg–Guinier focusing camera and $FeK_{\alpha 1}$ radiation ($\lambda = 1{\cdot}93597$ Å), to eliminate the fluorescent scattering caused by Dy-containing materials with the usual Cu radiation. Films were measured with an automatic LS20 LineScanner using the programme SCANPI and accompanying software. Unit cell definition was attempted using the indexing programme TREOR, but in spite of good quality data, these results were found, in general, to be inconsistent because of the pseudo-symmetry discussed above which resulted in numerous close overlaps. Unit cell refinement was therefore carried out based on the known europium aluminate ($Eu_4Al_2O_9$) structure, using the programmes PIRUM and PURUM, the latter enabling weightings to be assigned for overlapping reflections. Since the end members of the $Dy_4Si_2O_7N_2$–$Dy_4Al_2O_9$ series index well in the monoclinic space group $P2_1/a$, the associated absence rules were rigidly adhered to for the indexing of intermediate compositions.

Yttrium-containing samples used for preliminary indexing of the X-ray patterns were obtained either by hot-pressing at 1700°C, in the case of $Y_4Si_2O_7N_2$, or by firing at ~2000°C by means of an oxyacetylene blow torch. X-ray data were gathered using CuK_{α_1} radiation; the rest of the procedure was as described above.

In the course of this work, many other samples were prepared in addition to the ones used for data points included in results tables and graphs. One interesting observation was the range of colours obtained in shades of grey, varying from homogeneous light grey or dark grey to merely a contrast between the outer and inner material in the pellet, which could be either light/dark or

Table 2. X-ray diffraction data for yttrium YAM phase, $Y_4Al_2O_9$

h k l	d_{obs}	I_{obs}	*h k l*	d_{obs}	I_{obs}	*h k l*	d_{obs}	I_{obs}	*h k l*	d_{obs}	I_{obs}
1 1 0	7·4330	23	$\bar{2}$ 3 2	2·4576	7	$\bar{2}$ 0 4	1·8431	29	$\bar{5}$ 1 4	1·6038	2
0 0 1	6·9918	1	$\bar{4}$ 1 2	2·4568		2 4 2	1·8303	23	5 1 2	1·5767	12
2 0 0	5·2713	2	$\bar{2}$ 0 3	2·4388	<1	$\bar{4}$ 4 2	1·8169	29	6 3 0	1·5693	1
0 2 0			$\bar{2}$ 1 3	2·3744	<1	3 5 1	1·8137	1	1 2 4	1·5667	15
$\bar{2}$ 0 1	5·0488	<1	4 2 0	2·3546	1	4 1 2			0 3 4	1·5624	23
2 1 0	4·7073	29	2 2 2	2·2999	<1	5 3 0	1·8045	<1	3 6 0		
1 2 0	4·6870	3	1 3 2	2·2923	8	3 5 0	1·7982	3	0 6 2	1·5599	2
$\bar{2}$ 1 1	4·5502	3	$\bar{3}$ 3 2	2·2749	7	0 5 2	1·7961	<1	$\bar{7}$ 1 2		
0 2 1	4·1919	1	$\bar{4}$ 2 2			$\bar{6}$ 1 2	1·7918	7	$\bar{2}$ 6 2	1·5583	2
2 2 0	3·7140	2	$\bar{3}$ 1 3	2·2563	1	$\bar{2}$ 5 2			$\bar{4}$ 3 4	1·5515	10
2 0 1	3·6863	<1	$\bar{2}$ 2 3	2·2090	1	$\bar{3}$ 1 4	1·7853	<1	$\bar{3}$ 5 3		
0 0 2	3·4971	<1	$\bar{3}$ 3 1	2·1864	<1	$\bar{5}$ 2 3	1·7784	<1	$\bar{5}$ 2 4	1·5504	15
$\bar{1}$ 1 2	3·4756	<1	$\bar{5}$ 1 1	2·1761	1	6 0 0	1·7574	1	5 2 2	1·5256	1
2 1 1			$\bar{1}$ 4 2	2·1339	1	0 6 0	1·7439	<1	$\bar{7}$ 2 2	1·5109	<1
$\bar{2}$ 0 2	3·4664	<1	2 1 4			6 1 0	1·7324	5	$\bar{6}$ 4 1	1·5099	<1
3 1 0	3·3310	27	3 1 2			1 5 2	1·7240	13	$\bar{2}$ 4 4	1·5069	8
0 1 2	3·3163	1	$\bar{3}$ 2 3	2·1127	<1	0 1 4			1 4 4	1·4940	1
$\bar{2}$ 1 2	3·2915	1	1 1 3	2·0942	1	$\bar{3}$ 5 2	1·7167	12	6 4 2		
1 2 2	3·0155	100	$\bar{2}$ 4 2	2·0877	1	$\bar{3}$ 2 4	1·7122	<1	$\bar{3}$ 4 4	1·4893	<1
3 2 0	2·9176	70	$\bar{5}$ 1 2			$\bar{4}$ 1 4	1·7092	1	$\bar{6}$ 1 4	1·4854	5
2 3 0	2·9073	40	5 1 0	2·0657	23	4 4 1	1·7021	<1	5 5 0		
0 2 2			2 3 2			0 6 1	1·6928	1	1 7 0	1·4805	2
2 2 2	2·8874	9	1 5 0	2·0528	3	$\bar{6}$ 0 3	1·6841	1	$\bar{5}$ 3 4	1·4714	<1
$\bar{3}$ 1 2			$\bar{4}$ 3 2	2·0457	8	3 4 2	1·6653	<1	6 4 0	1·4584	<1
4 0 0	2·6355	<1	1 4 2	1·9833	2	$\bar{5}$ 3 3	1·6628	<1	4 6 0	1·4545	1
0 4 0	2·6165	8	$\bar{5}$ 2 2	1·9719	2	$\bar{6}$ 1 3			5 3 2	1·4502	<1
2 0 2	2·5614	10	$\bar{3}$ 4 2			2 6 0	1·6558	1	7 2 0	1·4468	<1
1 4 0	2·5392	5	5 2 0	1·9561	<1	$\bar{5}$ 4 2	1·6518	<1	2 7 0	1·4383	7
$\bar{4}$ 0 2	2·5255	11	2 5 0	1·9464	1	1 6 1			1 7 1	1·4348	<1
$\bar{3}$ 3 1	2·5182	<1	1 5 1	1·9383	<1	4 5 0	1·6376	1	$\bar{4}$ 1 5	1·4255	<1
2 1 2	2·4879	2	2 0 3	1·9199	<1	4 3 2	1·6285	5	$\bar{3}$ 2 5	1·4148	<1
3 3 0	2·4751	3	$\bar{4}$ 4 1	1·9033	1	1 1 4	1·6221	3	6 0 2	1·4006	<1
3 2 1	2·4695	4	4 3 1	1·8860	<1	$\bar{6}$ 3 2	1·6129	6			
0 3 2			$\bar{5}$ 3 1	1·8760	<1	$\bar{3}$ 3 4	1·6075	2			

S.G. $P2_1/a$ $a = 11{\cdot}1224(6)$, $b = 10{\cdot}4663(5)$, $c = 7{\cdot}3743(4)$Å; $\beta = 108{\cdot}563(4)°$

dark/light, respectively. In general, where a contrast was obtained, the darker material was the inner region, but in a few cases the reverse was true. This was the case for samples for which the intended temperature was greatly exceeded for a short time, causing the outside only to reach the higher temperature before equilibrating. For the remaining samples, the proportion of light to dark material varied according to composition and temperature in relation to the eutectic (believed to be near the low x end of the range); X-ray photographs were taken of both regions and close examination of the diffraction patterns revealed that there was no particular relationship between colour and J-phase type; however it was surmised that the darker regions probably contained more liquid phase enabling better densification to occur. Colour change was also found to be very sensitive to even the small changes in temperature caused by aging of the furnace element during the course of the work. These observations provide strong evidence that in the temperature range 1700–1750°C structural changes were taking place in these materials.

3 Results

The indexing of the diffraction patterns of $Dy_4Si_2O_7N_2$ and $Dy_4Al_2O_9$ was carried out by comparison with the related compounds $Y_4Si_2O_7N_2$ and $Y_4Al_2O_9$. The data indexed well (Tables 4 and 7), showing that the structures are similar. This is to be expected because the atomic sizes of Dy^{3+} and Y^{3+} are almost identical. X-ray data for $Dy_4Al_2O_9$ and $Y_4Al_2O_9$ have already been published (ICDD Refs 46-367 and 34-368, respectively) and differ only slightly in the designation of weak lines compared with the yttrium analogue in the present work.

In the present study, compositions in the $Dy_4Si_{2-x}Al_xO_{7+x}N_{2-x}$ series were prepared with x increasing from 0 to 2 in steps of 0·1. Because of the similarity in structure between the two end-members of the yttrium J-phase series, it was originally supposed that a single solid solution existed between $x = 0$ and $x = 2$, but the noticeable departure of mid-series b measurements from the straight line joining $Y_4Si_2O_7N_2$ and $Y_4Al_2O_9$[9] cast doubt on this conclusion and has subsequently

Table 3. X-ray diffraction data for yttrium J-phase, $Y_4Si_2O_7N_2$

h k l	d_{obs}	I_{obs}	*h k l*	d_{obs}	I_{obs}	*h k l*	d_{obs}	I_{obs}	*h k l*	d_{obs}	I_{obs}
1 1 0	7·2759	32	$\bar{4}$ 1 2	2·4311	6	2 4 2	1·8160	30	0 3 4	1·5822	18
0 0 1	7·1139	1	$\bar{2}$ 1 3			$\bar{4}$ 4 2	1·8068	28	$\bar{6}$ 3 2	1·5795	< 1
0 1 1	5·8819	< 1	3 3 0	2·4198	1	0 5 2	1·8024	9	1 2 4	1·5775	35
0 2 0	5·2326	< 1	3 2 1	2·3994	3	$\bar{3}$ 5 1			$\bar{4}$ 3 4	1·5739	10
2 0 0	5·0460	4	$\bar{4}$ 2 1	2·3871	1	$\bar{2}$ 5 2	1·7998	< 1	0 6 2	1·5651	27
$\bar{2}$ 0 1	5·0037	< 1	$\bar{2}$ 4 1	2·3175	< 1	$\bar{5}$ 3 2	1·7907	1	$\bar{3}$ 6 1		
1 2 0	4·6473	2	$\bar{3}$ 1 3	2·2937	< 1	2 2 3			$\bar{3}$ 5 3	1·5639	< 1
1 1 1	4·5452	23	1 3 2	2·2913	10	4 0 2	1·7861	< 1	$\bar{6}$ 2 6		
2 1 0			$\bar{3}$ 3 2	2·2788	8	3 5 0	1·7761	6	3 6 0	1·5475	3
2 1 1	4·5169	2	2 2 2	2·2730	1	$\bar{5}$ 2 3			$\bar{2}$ 4 4	1·5320	10
0 2 1	4·2164	1	$\bar{4}$ 2 2	2·2549	1	$\bar{6}$ 0 2	1·7713	< 1	5 1 2	1·5244	6
1 2 1	3·6322	6	$\bar{2}$ 2 3			4 1 2	1·7604	7	6 0 1	1·5224	< 1
2 2 0			$\bar{1}$ 4 2	2·1508	7	0 1 4	1·7500	5	$\bar{1}$ 4 4	1·5164	< 1
$\bar{2}$ 2 1	3·6149	< 1	$\bar{3}$ 2 3	2·1456	< 1	$\bar{6}$ 1 2	1·7467	10	$\bar{7}$ 1 2		
$\bar{1}$ 1 2	3·5539	< 1	3 3 1	2·1351	< 1	5 3 0			6 3 0	1·5134	14
0 0 2			2 4 1	2·1103	< 1	0 6 0	1·7439	< 1	$\bar{3}$ 4 4		
$\bar{2}$ 0 2	3·5324	< 1	1 1 3	2·1027	2	$\bar{4}$ 1 4	1·7394	2	6 1 1	1·5059	1
2 1 1	3·3821	2	$\bar{2}$ 4 2			1 5 2	1·7231	23	$\bar{6}$ 0 4		
0 1 2	3·3641	1	$\bar{4}$ 1 3	2·0846	< 1	$\bar{3}$ 5 2	1·7179	20	$\bar{6}$ 3 3	1·5038	< 1
$\bar{2}$ 1 2	3·3464	< 1	3 1 2	2·0636	< 1	0 6 1	1·6928	1	2 1 4		
1 3 0	3·2980	1	1 5 0	2·0486	< 1	6 0 0	1·6803	2	$\bar{7}$ 1 1	1·5013	< 1
3 1 0	3·2011	36	3 1 2			2 3 3	1·6717	< 1	$\bar{6}$ 1 4	1·4901	< 1
$\bar{1}$ 2 2	3·0679	100	$\bar{2}$ 3 2	2·0445	22	$\bar{4}$ 2 4			$\bar{5}$ 3 4	1·4850	< 1
0 2 2	2·9386	15	$\bar{4}$ 3 2	2·0315	13	$\bar{6}$ 0 3	1·6649	1	1 7 0	1·4784	6
$\bar{2}$ 2 2	2·9273	29	4 2 1	1·9910	< 1	6 1 0	1·6586	7	5 2 2		
1 1 2	2·9177	< 1	5 1 0	1·9800	37	1 6 1	1·6477	4	4 4 2	1·4752	1
$\bar{6}$ 1 2	2·8938	13	$\bar{3}$ 4 2	1·9744	6	2 6 0			$\bar{6}$ 4 2	1·4676	2
2 3 0	2·8694	52	3 2 2	1·9537	1	$\bar{2}$ 6 1	1·6460	< 1	$\bar{4}$ 1 5	1·4575	2
3 2 0	2·8309	67	$\bar{3}$ 3 3	1·9506	< 1	$\bar{6}$ 1 3			$\bar{7}$ 2 1	1·4565	< 1
1 2 2	2·6267	< 1	1 5 1	1·9322	1	3 4 2	1·6409	1	5 5 0	1·4519	10
0 4 0	2·6161	10	2 5 0			$\bar{3}$ 3 4	1·6370	< 1	4 6 0	1·4332	13
1 4 0	2·5311	12	2 0 3	1·9055	1	1 1 4	1·6338	5	1 7 1		
2 0 2	2·5241	17	$\bar{2}$ 0 4	1·8898	49	$\bar{5}$ 4 2	1·6317	< 1	2 7 0		
$\bar{4}$ 0 2	2·4998	19	5 2 0	1·8806	1	$\bar{5}$ 1 4	1·6206	4	$\bar{4}$ 6 2	1·4305	1
$\bar{2}$ 0 3			$\bar{4}$ 4 1	1·8726	2	4 5 0	1·6098	2	6 4 0	1·4138	2
0 3 2	2·4883	4	4 3 1	1·8321	2	$\bar{4}$ 5 2	1·6041	< 1	$\bar{7}$ 3 2	1·4012	1
2 3 2	2·4808	3	$\bar{3}$ 1 4	1·8260	1	5 4 0	1·5968	< 1			
2 1 2	2·4535	6	$\bar{5}$ 3 1			4 3 2	1·5895	12			

S.G. P2,a $a = 10{\cdot}7334(10)$, $b = 10{\cdot}4621(10)$, $c = 7{\cdot}5627(9)$ Å; $\beta = 110{\cdot}081(9)^\circ$

never been satisfactorily explained. Examination of the X-ray patterns of the Dy J-phases showed quite clearly that more than one type of cuspidine structure was present; in fact, no fewer than five distinct structural modifications have been identified. Unit cell parameters for all structures are listed in Table 5 and the ranges of composition for each series are shown in Fig. 5. For the purpose of discussion the structures are labelled 1–5 and an example of each pattern is shown in Fig. 6(a)–(e), respectively, for comparison.

Series 1 runs from $x = 0$ to $x = 0{\cdot}4$ and indexes well in space group $P2_1/a$, with almost every calculated line visible on the X-ray pattern; Table 4 lists all permitted reflections up to 50° 2θ (2·27 Å) and it can be seen that, in general, lines with l even are strong, while those with l odd are weak. Also, there is a significant separation in θ between hk0 and the corresponding kh0 reflections as seen in the regions 21–22° and 24–25° 2θ [Fig. 6(a)], where 020, 200 and 120, 210 are clearly defined doublets.

Series 2 extends from $x = 0{\cdot}5$ up to $x = 1{\cdot}5$ and in Fig. 5 it can be seen that there is a significant drop in the value of b between $x = 0{\cdot}4$ and $x = 0{\cdot}6$, consistent with the findings of previous researchers; the poor fit for the result at $x = 0{\cdot}5$ is due to the structural change taking place at this composition. An obvious feature concerning Series 2 [Table 6, Fig. 6(b)] is the presence of extra lines at ~5·86 Å and 5·06 Å (19° and 22° 2θ). These lines index as 011 and $\bar{2}01$, respectively, and are abnormally large in intensity compared with odd l lines in the other series. This is the only series in which hkl reflections with l odd are of significant intensity, other examples being 031, $\bar{1}31$ (36°) and 311 (42·6°). The intensities of these weak reflections in Series 2 systematically decrease with increasing x-value.

Series 3 extends from $x = 1{\cdot}6$ to $Dy_4Al_2O_9$ at $x = 2{\cdot}0$ following a further break in continuity at about $x = 1{\cdot}5$. At this end the X-ray pattern matches well with that established for $Y_4Al_2O_9$. Again,

Table 4. X-ray diffraction data for Dy J-phase Series 1 showing all permitted reflections in space group $P2_1/a$

	x = 0				x = 0·4			
h k l	d_{calc}	d_{obs}	$2\theta_{obs}$	I_{obs}	d_{calc}	d_{obs}	$2\theta_{obs}$	I_{obs}
1 1 0	7·2875	7·2670	15·31	40	7·3170	7·3429	15·15	50
0 0 1	7·1400	7·1326	15·60	1	7·1330	7·1673	15·52	1
0 1 1	5·9038	—			5·9003	5·8801	18·88	<1
$\bar{1}$ 1 1	5·8801	—			5·8762			
0 2 0	5·2487	5·2392	21·29	6	5·2501	5·2600	21·21	6
2 0 0	5·0625	5·0548	22·08	7	5·1009	5·1082	21·85	7
2 0 1	5·0260	5·0201	22·23	1	5·0415	5·0465	22·12	1
1 2 0	4·6598	4·6533	24·01	11	4·6682	4·6741	23·90	13
1 1 1	4·5658	4·5547	24·54	42	4·5785	4·5935	24·33	44
2 1 0	4·5599				4·5882			
$\bar{2}$ 1 1	4·5332	4·5265	24·70	2	4·5448	4·5486	24·57	5
0 2 1	4·2290	4·2251	26·49	2	4·2283	4·2313	26·45	2
$\bar{1}$ 2 1	4·2203				4·2193			
1 2 1	3·6468	3·6420	30·83	10	3·6536	3·6600	30·67	9
2 2 0	3·6438				3·6585			
$\bar{2}$ 2 1	3·6301	3·6288	30·94	1	3·6364	3·6375	30·87	1
2 0 1	3·5879	—			3·6077	3·6093	31·13	2
$\bar{1}$ 1 2	3·5749	3·5673	31·49	2	3·5680	3·5665	31·50	3
0 0 2	3·5700				3·5665			
$\bar{2}$ 0 2	3·5491	3·5483	31·66	3	3·5452	3·5439	31·70	5
2 1 1	3·3951	3·3933	33·15	2	3·4119	3·4130	32·95	1
0 1 2	3·3799	3·3782	33·30	4	3·3770	3·3762	33·32	6
$\bar{3}$ 1 1	3·3727				3·3887	—		
$\bar{2}$ 1 2	3·3622	3·3613	33·47	4	3·3589	3·3579	33·51	6
1 3 0	3·3072	3·3061	34·05	8	3·3106	3·3124	33·98	8
3 1 0	3·2130	3·2121	35·08	37	3·2352	3·2358	34·81	34
0 3 1	3·1421	—			3·1422	—		
$\bar{1}$ 3 1	3·1385	—			3·1385	—		
$\bar{1}$ 2 2	3·0792	3·0786	36·65	100	3·0749	3·0740	36·71	100
2 2 1	2·9620	—			2·9734	—		
0 2 2	2·9519	2·9513	38·29	17	2·9502	2·9492	38·32	16
$\bar{3}$ 2 1	2·9471				2·9579	—		
$\bar{2}$ 2 2	2·9401	2·9388	38·46	9	2·9381	2·9350	38·51	37
1 1 2	2·9318	2·9320	38·56	34	2·9356			
$\bar{3}$ 1 2	2·9088	2·9085	38·88	29	2·9120	2·9102	38·85	29
1 3 1	2·8799	2·8784	39·30	53	2·8836	2·8862	39·19	50
2 3 0	2·8785				2·8860			
$\bar{2}$ 3 1	2·8717				2·8751	2·8730	39·38	1
3 2 0	2·8388	2·8390	39·87	70	2·8542	2·8543	39·65	68
$\bar{4}$ 0 1	2·6959	—			2·7126	2·7116	41·83	1
1 2 2	2·6392	2·6394	43·03	1	2·6421	2·6414	43·00	1
3 1 1	2·6257	2·6249	43·28	26	2·6415			
0 4 0	2·6243				2·6250	2·6251	43·28	27
$\bar{3}$ 2 2	2·6224				2·6249			
$\bar{4}$ 1 1	2·6111	—			2·6264			
$\bar{1}$ 3 2	2·5747	—			2·5725	—		
1 4 0	2·5404	2·5403	44·80	8	2·5422	2·5423	44·76	43
2 0 2	2·5353	2·5360	44·88	37	2·5438			
4 0 0	2·5312				2·5504	—		
$\bar{4}$ 0 2	2·5130	2·5136	45·30	31	2·5208	2·5189	45·20	32
$\bar{2}$ 0 3	2·5124				2·5071	—		
2 3 1	2·5051	—			2·5121	—		
0 3 2	2·4989	2·4993	45·57	7	2·4981	2·4972	45·61	9
$\bar{3}$ 3 1	2·4960				2·5028	—		
$\bar{2}$ 3 2	2·4917	2·4927	45·70	7	2·4907	2·4893	45·77	7
2 1 2	2·4644	2·4648	46·25	11	2·4723	2·4715	46·12	9
0 4 1	2·4632				2·4635	2·4629	46·29	1
$\bar{1}$ 4 1	2·4615				2·4617			
4 1 0	2·4607				2·4784	2·4770	46·01	2
$\bar{1}$ 1 3	2·4485	2·4444	46·66	10	2·4438	—		
$\bar{4}$ 1 2	2·4439				2·4511	2·4493	46·56	14
$\bar{2}$ 1 3	2·4434				2·4386	2·4387	46·77	3
3 3 0	2·4292	2·4300	46·95	2	2·4390			
3 2 1	2·4093	2·4099	47·36	4	2·4216	2·4209	47·14	4

Table 4.—*contd.*

	x = 0				x = 0·4			
h k l	d_{calc}	d_{obs}	$2\theta_{obs}$	I_{obs}	d_{calc}	d_{obs}	$2\theta_{obs}$	I_{obs}
$\bar{4}$ 2 1	2·3980	2·3987	47·60	2	2·4099	2·4086	47·39	2
0 0 3	2·3800	—			2·3777	—		
1 4 1	2·3307				2·3328	—		
2 4 0	2·3299	2·3270	49·16	1	2·3341	—		
$\bar{2}$ 4 1	2·3263				2·3283	2·3278	49·14	2
0 1 3	2·3211	—			2·3190	—		
$\bar{3}$ 1 3	2·3082	2·3086	49·58	3	2·3058	2·3018	49·74	15
1 3 2	2·3006	2·3016	49·74	11	2·3027			
$\bar{3}$ 3 2	2·2894	2·2904	50·00	13	2·2912	2·2895	50·02	14
2 2 2	2·2829	2·2837	50·16	2	2·2892			
4 2 0	2·2800				2·2941	—		
$\bar{1}$ 2 3	2·2702	2·2672	50·55	2	2·2665	2·2605	50·71	1
$\bar{2}$ 2 3	2·2662				2·2624			
$\bar{4}$ 2 2	2·2666				2·2724	2·2704	50·47	1

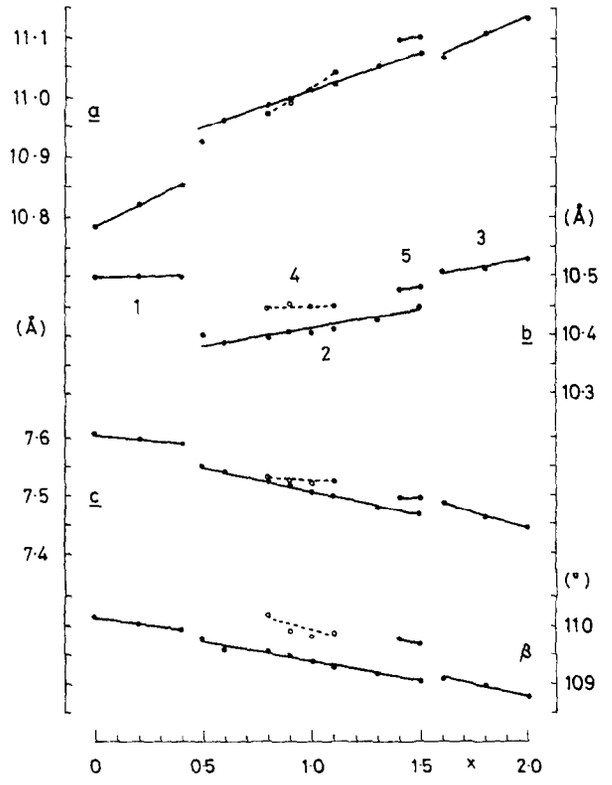

Fig. 5. Variation in unit cell dimensions with x, for $x = 0-2$ along the $Dy_4Si_{2-x}Al_xO_{7+x}N_{2-x}$ line.

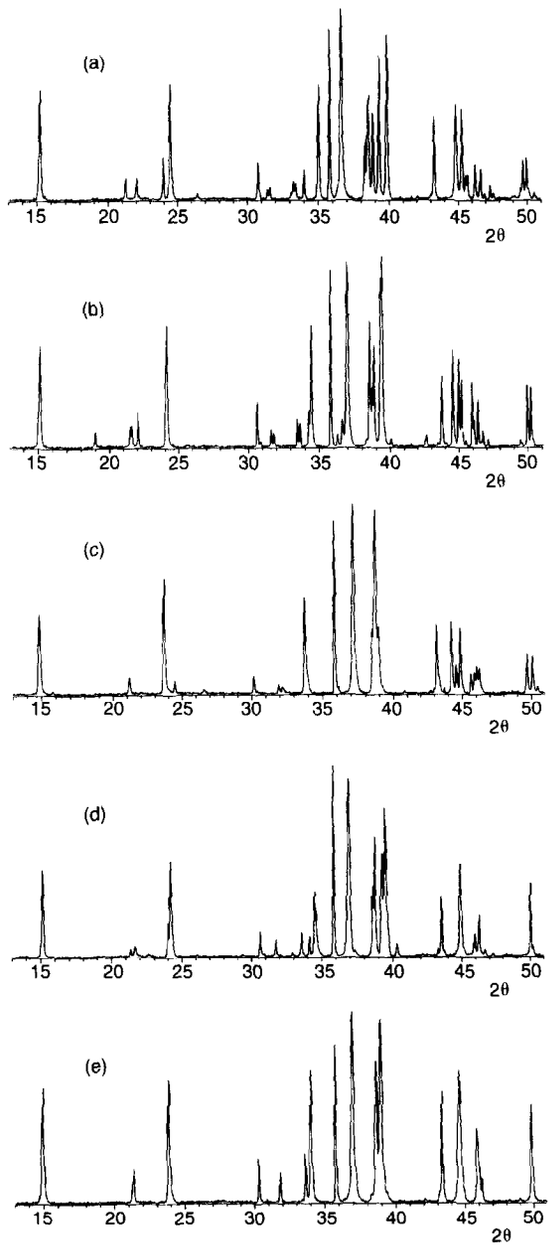

Fig. 6. Selected X-ray diffraction patterns for Dy J-phase compounds: (a) series 1, $x = 0$; (b) series 2, $x = 0·6$; (c) series 3, $x = 2·0$; (d) series 4, $x = 0·8$; (e) series 5, $x = 1·4$.

it can be seen from Table 7 that reflections with 1 odd are either absent or very weak. In contrast to the pattern at $x = 0$ where hk0 and corresponding kh0 reflections are of comparable intensity, at $x = 2$, although the separation of these pairs is quite measurable, only one is strong, while the other is insignificant. However, a notable inconsistency to this fact appears at 2·89 Å (39°), where a strong line is indexed by the refinement as 131. This is in agreement with the indexing of the ICDD pattern for $Dy_4Al_2O_9$, but since there are several almost overlapping lines with 1 even (230, $\bar{3}$12, 320)

Table 5. Unit cell parameters for Dy J-phase Series 1–5

Series 1				
	$x=0$	$x=0{\cdot}2$	$x=0{\cdot}4$	
aÅ	10·7841(22)	10·8202(22)	10·8522(35)	
bÅ	10·4973(21)	10·5007(24)	10·5002(35)	
cÅ	7·6048(16)	7·5958(15)	7·5878(28)	
$\beta°$	110·135(14)	110·042(15)	109·937(29)	
VÅ^3	808·28	810·77	812·81	
Series 2				
	$x=0{\cdot}5$	$x=0{\cdot}6$	$x=0{\cdot}8$	$x=0{\cdot}9$
aÅ	10·9244(74)	10·9598(25)	10·9873(41)	10·9966(24)
vÅ	10·3994(73)	10·3886(22)	10·3948(37)	10·4060(25)
cÅ	7·5489(53)	7·5359(19)	7·5225(26)	7·5177(17)
$\beta°$	109·768(53)	109·589(18)	109·525(27)	109·466(18)
VÅ^3	807·06	808·35	809·74	811·08
	$x=1{\cdot}0$	$x=1{\cdot}1$	$x=1{\cdot}3$	$x=1{\cdot}5$
aÅ	11·0111(24)	11·0184(43)	11·0514(19)	11·0733(62)
bÅ	10·405(20)	10·4092(37)	10·4263(17)	10·4487(53)
cÅ	7·5074(15)	7·4967(30)	7·4803(12)	7·4676(43)
$\beta°$	109·388(15)	109·269(30)	109·150(12)	109·040(45)
VÅ^3	811·65	811·36	814·22	816·74
Series 3				
	$x=1{\cdot}6$	$x=1{\cdot}8$	$x=2{\cdot}0$	
aÅ	11·0682(79)	11·1097(47)	11·1316(18)	
bÅ	10·5069(65)	10·5110(46)	10·5278(19)	
cÅ	7·4846(54)	7·4640(28)	7·4422(13)	
$\beta°$	109·068(48)	108·958(30)	108·780(12)	
VÅ^3	822·64	824·32	825·73	
Series 4				
	$x=0{\cdot}8$	$x=0{\cdot}9$	$x=1{\cdot}0$	$x=1{\cdot}1$
aÅ	10·9740(68)	10·9940(60)	11·0171(82)	11·0406(107)
bÅ	10·4473(58)	10·4546(67)	10·4486(174)	10·4496(100)
cÅ	7·5305(41)	7·5239(56)	7·5198(21)	7·5231(103)
$\beta°$	110·164(52)	109·900(52)	109·796(151)	109·857(104)
VÅ^3	810·45	813·14	814·47	816·33
Series 5				
	$x=1{\cdot}4$ (m/c)	$x=1{\cdot}4$ (o/r)	$x=1{\cdot}5$ (m/c)	$x=1{\cdot}5$ (o/r)
aÅ	11·0984	10·4053(139)	11·1019	10·4424(55)
bÅ	10·4774	10·4872(169)	10·4800	10·4972(55)
cÅ	7·4951	7·4988(142)	7·4891	7·4988(45)
$\beta°$	109·759		109·660	
VÅ^3	820·23	818·29	820·55	821·99

at this point, it would seem more likely that the 2·89 Å line should be indexed as one of these.

Series 4 is observed in the range $x = 0{\cdot}8$ to $x = 1{\cdot}1$. X-ray patterns appear to consist of a major product and a small amount of an additional J-phase; neither of these corresponded to the previously identified series, even allowing for the fact that $x = 0{\cdot}8$ represents the starting composition and the fired products may not be of exactly the same composition. Table 8 shows X-ray diffraction data for the end points of the series, $x = 0{\cdot}8$ and $x = 1{\cdot}1$. Refinement was carried out as before, using PIRUM and PURUM, adhering also to the conditions of space group $P2_1/a$. In this case agreement between observed and calculated positions for designated hkl lines was very poor, and although almost overlapping, pairs of reflections corresponding to the alternative unit cells e.g. $002/\bar{2}02$, $112/\bar{3}12$ were, in the main, reversed in position by the refinement programmes. This phenomenon suggests that there is a significant change in a/b ratio between the J-phases of Series 2 and 4. This point can best be illustrated by plotting calculated unit cell volumes as a function of composition (Fig. 7) which shows that the ends of the compositional range (Series 1 and 3) appear to be structurally related, whilst the region between $x = 0{\cdot}5$ and $x = 1{\cdot}5$ shows discontinuities at either end, indicative of a structural change.

Series 5, although referred to as such, is of very limited extent, and describes a region in the compositional range $x = 1{\cdot}4 - 1{\cdot}5$ in which the X-ray diffraction patterns become significantly simplified so as to index apparently with orthorhombic

Table 6. X-ray diffraction data for Dy J-phase Series 2

	x = 0·6				x = 1·0				x = 1·5			
h k l	d_{calc}	d_{obs}	$2\theta_{obs}$	I_{obs}	d_{calc}	d_{obs}	$2\theta_{obs}$	I_{obs}	d_{calc}	d_{obs}	$2\theta_{obs}$	I_{obs}
1 1 0	7·3234	7·3374	15·16	45	7·3510	7·3425	15·15	39	7·3950	7·3948	15·04	42
0 1 1	5·8617	5·8694	18·98	5	5·8544	5·8505	19·05	35·8493	5·8437	19·07		2
0 2 0	5·1943	5·1973	21·47	6	5·2025	5·1914	21·49	8	5·2243	5·2307	21·33	8
2 0 0	5·1627	5·1659	21·60	7	5·1933				5·2338			
$\bar{2}$ 0 1	5·0596	5·0630	22·04	9	5·0660	5·0610	22·05	6	5·0692	5·0681	22·02	3
1 2 0	4·6402	4·6415	24·07	14	4·6516	4·6456	24·05	46	4·6745	4·6791	23·88	48
2 1 0	4·6233	4·6252	24·16	44	4·6467				4·6795			
1 1 1	4·5820	—			4·5896	4·5889	24·36	2	4·6036	—		
$\bar{2}$ 1 1	4·5488	4·5526	24·55	1	4·5548	4·5697	24·46	1	4·5608	4·5669	24·47	2
2 2 0	3·6617	3·6620	30·65	12	3·6755	3·6746	30·55	9	3·6975	3·6998	30·33	8
1 2 1	3·6411	3·6367	30·87	2	3·6471	3·6456	30·80	1	3·6597	3·6602	30·67	1
2 0 1	3·6358				3·6498				3·6703	3·6750	30·54	< 1
0 0 2	3·5499	3·5513	31·63	5	3·5408	3·5403	31·74	3	3·5295	3·5290	31·84	4
$\bar{1}$ 1 2	3·5420				3·5308	3·5183	31·94	3	3·5159	3·5157	31·96	< 1
$\bar{2}$ 0 2	3·5292	3·5304	31·83	4	3·5194				3·5037	3·5074	32·04	3
0 1 2	3·3592	3·3600	33·49	7	3·3521	3·3527	33·56	5	3·3439	3·3433	33·66	6
$\bar{2}$ 1 2	3·3417	3·3425	33·67	7	3·3339	3·3331	33·76	4	3·3219	—		
1 3 0	3·2832	3·2828	34·30	12	3·2898	3·2857	34·27	44	3·3095	3·3102	34·01	47
3 1 0	3·2672	3·2665	34·48	42	3·2851				3·3048			
0 3 1	3·1124	3·1090	36·28	4	3·1148	3·1122	36·24	2	3·1234	3·1242	36·01	2
$\bar{1}$ 3 1	3·1089				3·1112				3·1189			
$\bar{1}$ 2 2	3·0499	3·0508	37·00	100	3·0440	3·0438	37·09	100	3·0376	3·0355	37·19	68
2 2 1	2·9786	2·9806	37·90	< 1	2·9879	—			3·0032	—		
1 1 2	2·9324	2·9319	38·56	44	2·9321	2·9318	38·56	36	2·9333	2·9326	38·55	36
0 2 2	2·9308				2·9272				2·9247	2·9192	38·73	3
$\bar{2}$ 2 2	2·9192	2·9188	38·74	15	2·9151	2·9154	38·78	4	2·9099	—		
$\bar{3}$ 1 2	2·9092	2·9090	38·87	32	2·9079	2·9075	38·89	31	2·9038			
2 3 0	2·8759	2·8747	39·35	49	2·8843	2·8831	39·23	98	2·8995	2·9021	38·97	100
3 2 0	2·8691	2·8681	39·45	68	2·8823				2·9016			
1 3 1	2·8658				2·8705	—			2·8812	2·8847	39·21	4
3 1 1	2·6635	2·6630	42·63	4	2·6757	2·6748	42·43	3	2·6933	2·6942	42·11	2
$\bar{4}$ 1 1	2·6482	—			2·6595	—			2·6732	2·6676	42·55	7
1 2 2	2·6344	2·6334	43·13	< 1	2·6350	2·6355	43·10	1	2·6380	—		
4 0 0	2·5814	2·5811	44·05	2	2·5967	2·6009	43·70	26	2·6169	2·6172	43·41	3
0 4 0	2·5972	2·5961	43·78	26	2·6013				2·6122	2·6115	43·51	23
2 0 2	2·5527	2·5521	44·58	35	2·5570	2·5580	44·47	32	2·5641	2·5638	44·36	34
$\bar{1}$ 3 2	2·5496				2·5474	—			2·5468	2·5459	44·69	5
$\bar{4}$ 0 2	2·5298	2·5290	45·01	32	2·5330	2·5326	44·94	27	2·5346			
1 4 0	2·5187	2·5176	45·22	21	2·5233	2·5231	45·12	18	2·5344	2·5361	44·88	41
4 1 0	2·5052	2·5039	45·48	3	2·5194				2·5385			
2 3 1	2·5075				2·5142	—			2·5264	2·5243	45·10	1
3 3 1	2·4984	—			2·5046	—			2·5145	2·5155	45·26	2
0 3 2	2·4788	2·4782	45·98	20	2·4777	2·4780	45·99	7	2·4791	2·4787	45·97	9
2 1 2	2·4790				2·4831	2·4826	45·90	10	2·4902	2·4898	45·76	11
$\bar{2}$ 3 2	2·4718	2·4717	46·11	6	2·4704	2·4704	46·14	5	2·4701			
$\bar{4}$ 1 2	2·4580	2·4573	46·40	14	2·4611	2·4607	46·33	10	2·4632	2·4658	46·23	21
3 3 0	2·4411				2·4503	2·4508	46·53	5	2·4650			
0 4 1	2·4391	2·4398	46·75	5	2·4418	—			2·4498	2·4470	46·60	1
$\bar{1}$ 4 1	2·4374				2·4400	—			2·4476			
$\bar{2}$ 1 3	2·4221	2·4221	47·11	3	2·4139	2·4139	47·28	2	2·4022	2·3999	47·57	1

(apparently tetragonal[9]) symmetry. At $x = 1{\cdot}4$ in particular, there is negligible broadening of lines, indicating precise overlapping of reflections, inviting attempts to refine the unit cell using higher symmetry. Table 5 shows corresponding monoclinic and orthorhombic indexings for the sample at $x = 1{\cdot}4$ but there remains a distinct separation for pairs of orthorhombic-type reflections such as 020/200, 012/102 and 032/302, eliminating any possibility of the existence of a tetragonal cell. The calculated pattern for the monoclinic cell is obtained from 040, 200, 310, 02/002 and 12/012 reflections, but because of several precise overlaps, this was unrefinable. However, the equivalent orthorhombic unit cell did refine, albeit with greater standard deviations than in the other series due to the close proximity of hk0/kh0 pairs, as seen in Table 9. Another noticeable feature of the Series 5 patterns is that weak reflections for odd 1 disappear completely, indicating that the c axis can be halved. If there is an additional lattice point along the c axis, then Fig. 4 shows that it is quite feasible to have an orthorhombic cell with dimensions $a_m \sin\beta_m$, b_m, $c_m/2$,

Table 7. X-ray diffraction data for Dy J-phase Series 3

x = 1·6					x = 2·0					46-367
h k l	d_{calc}	d_{obs}	$2\theta_{obs}$	I_{obs}	*h k l*	d_{calc}	d_{obs}	$2\theta_{obs}$	I_{obs}	*h k l*
1 1 0	7·4132	7·4173	15·00	48	1 1 0	7·4482	7·4423	14·95	40	1 1 0
0 0 1	7·0739	—			0 0 1	7·0460	7·0422	15·80	1	
0 2 0	5·2535	5·2333	21·32	9	2 0 0	5·2695	5·2673	21·18	60	0 2 0*
2 0 0	5·2304				0 2 0	5·2639				
1 2 0	4·6947	4·6825	23·86	50	2 1 0	4·7122	4·7097	23·72	51	2 1 0
2 1 0	4·6823				1 2 0	4·7092				
$\bar{2}$ 1 1	4·5674	4·5720	24·45	1	$\bar{2}$ 1 1	4·5721	4·5698	24·46	5	$\bar{2}$ 1 1
0 2 1	4·2176	4·2203	26·52	1	0 2 1	4·2170	4·2156	26·55	2	
2 2 0	3·7066	3·7068	30·27	5	2 2 0	3·7241	3·7233	30·14	6	2 2 0
0 0 2	3·5369	3·5347	31·79	5	0 0 2	3·5230	3·5226	31·90	3	0 0 2
$\bar{1}$ 1 2	3·5251	3·5294	31·84	< 1	$\bar{1}$ 1 2	3·5081	—			
$\bar{2}$ 0 2	3·5099	3·5132	31·99	1	$\bar{2}$ 0 2	3·4943	3·4942	32·17	3	$\bar{2}$ 0 2
2 1 1	3·4657	3·4640	32·45	< 1	2 1 1	3·4811	—			
0 1 2	3·3521	3·3519	33·57	9	0 1 2	3·3409	3·3319	33·78	42	3 1 0
$\bar{2}$ 1 2	3·3291	3·3448	33·64	1	3 1 0	3·3324				
1 3 0	3·3211	—			1 3 0	3·3295				
3 1 0	3·3095	3·3082	34·03	35	$\bar{2}$ 1 2	3·3164	3·3153	33·95	3	
$\bar{1}$ 2 2	3·0479	3·0489	37·02	100	$\bar{1}$ 2 2	3·0384	3·0384	37·15	100	$\bar{1}$ 2 2
2 2 1	3·0092	—			2 2 1	3·0208	3·0209	37·38	5	
1 1 2	2·9387	2·9361	38·50	19	1 1 2	2·9369	2·9360	38·50	20	
0 2 2	2·9340				0 2 2	2·9278				
$\bar{2}$ 2 2	2·9185	2·9220	38·69	36	3 2 0	2·9220	2·9214	38·70	96	3 2 0
2 3 0	2·9101				2 3 0	2·9208				
$\bar{3}$ 1 2	2·9079	2·9050	38·93	81	$\bar{2}$ 2 2	2·9112	—			
3 2 0	2·9052				$\bar{3}$ 1 2	2·9038	2·9040	38·94	24	1 3 1*
1 3 1	2·8931	2·8934	39·09	57	1 3 1	2·8986				
$\bar{2}$ 3 1	2·8819	—			$\bar{2}$ 3 1	2·8865	2·8873	39·18	2	
$\bar{4}$ 0 1	2·7642	—			$\bar{4}$ 0 1	2·7787	2·7787	40·77	1	
3 1 1	2·6941	2·6947	42·10	1	3 1 1	2·7096	—			
1 2 2	2·6447	—			1 2 2	2·6444	2·6454	42·93	1	
0 4 0	2·6267	2·6275	43·23	15	4 0 0	2·6347	2·6320	43·16	24	0 4 0
$\bar{3}$ 2 2	2·6222	2·6162	43·43	17	0 4 0	2·6319				
4 0 0	2·6152				$\bar{3}$ 2 2	2·6201	2·6236	43·30	5	
2 0 2	2·5666	2·5642	44·36	16	2 0 2	2·5712	2·5714	44·23	27	2 0 2
$\bar{1}$ 3 2	2·5570	—			4 1 0	2·5559	2·5535	44·55	11	$\bar{1}$ 3 2
1 4 0	2·5476	2·5470	44·67	36	1 4 0	2·5535				
4 1 0	2·5378				$\bar{1}$ 3 2	2·5529				
$\bar{4}$ 0 2	2·5358	2·5368	44·86	27	2 3 1	2·5425	2·5375	44·85	26	$\bar{4}$ 0 2
2 3 1	2·5341				$\bar{4}$ 0 2	2·5379				
$\bar{3}$ 3 1	2·5216	2·5212	45·16	1	$\bar{3}$ 3 1	2·5289	2·5283	45·02	2	
2 1 2	2·4933	2·4902	45·75	8	2 1 2	2·4978	2·4979	45·60	8	2 1 2
0 3 2	2·4887				0 3 2	2·4863	2·4851	45·85	9	3 3 0
$\bar{2}$ 3 2	2·4792	2·4801	45·95	11	3 3 0	2·4827				
$\bar{2}$ 0 3	2·4736	2·4737	46·07	11	$\bar{2}$ 3 2	2·4761	2·4760	46·03	9	
3 3 0	2·4711				3 2 1	2·4748				
$\bar{4}$ 1 2	2·4650	2·4653	46·24	8	$\bar{4}$ 1 2	2·4672	2·4669	46·21	10	0 4 1*
3 2 1	2·4622				$\bar{4}$ 4 1	2·4631				
$\bar{1}$ 4 1	2·4601	2·4590	46·36	1	$\bar{2}$ 0 3	2·4598	2·4581	46·38	1	
$\bar{4}$ 2 1	2·4462	—			$\bar{4}$ 2 1	2·4573				
$\bar{2}$ 4 1	2·3325	2·3312	49·07	3	$\bar{2}$ 4 1	2·3365	—			

*hkl differs from present work.

consistent with the refined $x = 1{\cdot}4$ orthorhombic values of $a = 10{\cdot}405(14)$, $b = 10{\cdot}487(17)$, $c = 3{\cdot}749(7)$ Å. In this case the two orientations of the monoclinic cell shown in Fig. 4 have identical cells with dimensions $a = 11{\cdot}097(5)$, $b = 10{\cdot}477(5)$, $c = 7{\cdot}495(4)$ Å; $\beta = 109{\cdot}73(5)°$. The condition for an orthorhombic cell can be summarised as: $a_m\cos(180\text{-}\beta) = c_m/2$.

If the ratio $2a_m\cos(180-\beta)/c_m$ is plotted as a function of x (Fig. 8), it can be seen that the value of this ratio is always below 0·99 for Series 1, 2 and 3 and by extrapolation would never reach unity, whereas for Series 5, and indeed Series 4, this condition is more nearly satisfied. Figure 5 confirms that whereas the values of b and c for the orthorhombic phase are similar to Series 3 values, there is a discontinuity in a and β, which is further evidence for the Series 5 orthorhombic composition having the different symmetry. The similarity of $a_m\cos(180-\beta)/c_m$ for Series 4 and 5 suggests, in addition, that Series 4 is structurally related to Series 5; the fact that the

Table 8. X-ray diffraction data for Dy J-phase Series 4

	x = 0·8				x = 1·1			
h k l	d_{calc}	d_{obs}	$2\theta_{obs}$	I_{obs}	d_{calc}	d_{obs}	$2\theta_{obs}$	I_{obs}
1 1 0	7·3352	7·3336	15·17	36	7·3657	7·3693	15·10	37
0 2 0	5·2237	5·2243	21·36	3	5·2248	5·2347	21·31	3
2 0 0	5·1507	5·1532	21·65	5	5·1921	5·1836	21·52	5
$\bar{2}$ 0 1	5·0786	5·0796	21·97	< 1	5·0914	—		
1 2 0	4·6589	4·6576	23·99	9	4·6673	4·6674	23·94	7
2 1 0	4·6198	4·6192	24·19	46	4·6498	4·6448	24·06	45
2 2 0	3·6676	3·6663	30·62	7	3·6829	3·6813	30·49	8
$\bar{2}$ 2 1	3·6413	3·6526	30·74	< 1	3·6464	—		
1 2 1	3·6381	3·6329	30·91	< 1	3·6484	—		
$\bar{1}$ 1 2	3·5422				3·5392			
$\bar{2}$ 0 2	3·5383	3·5405	31·73	5	3·5354	3·5364	31·77	6
0 0 2	3·5345				3·5379			
$\bar{3}$ 1 1	3·4183	3·4171	32·91	1	3·4328	—		
2 1 1	3·4139				3·4357	—		
$\bar{2}$ 1 2	3·3514	3·3539	33·55	8	3·3489	3·3497	33·59	9
0 1 2	3·3480				3·3510			
1 3 0	3·2990	3·2994	34·12	6	3·3024	3·3055	34·06	6
3 1 0	3·2621	3·2625	34·52	27	3·2858	3·2799	34·33	35
$\bar{1}$ 2 2	3·0544	3·0577	36·91	100	3·0527	3·0544	36·95	93
$\bar{2}$ 2 2	2·9295	2·9307	38·57	22	2·9281	2·9287	38·60	12
0 2 2	2·9273				2·9295			
$\bar{3}$ 1 2	2·9208	2·9208	38·71	37	2·9230	2·9223	38·69	43
1 1 2	2·9164	2·9115	38·84	2	2·9258			
2 3 0	2·8849	2·8847	39·21	45	2·8926	2·8915	39·12	35
1 3 1	2·8705	2·8688			2·8758	—		
3 2 0	2·8694		39·44	79	2·8856	2·8830	39·24	100
$\bar{3}$ 2 2	2·6288	2·6287	43·21	2	2·6305	2·6309	43·18	2
1 2 2	2·6256				2·6326			
0 4 0	2·6118	2·6120	43·50	10	2·6124	2·6156	43·44	24
$\bar{1}$ 3 2	2·5566	2·5511	44·60	2	2·5557			
$\bar{4}$ 0 2	2·5393	2·5383	44·83	39	2·5485	2·5432	44·74	61
2 0 2	2·5350	2·5327	44·94	9	2·5457			
1 4 0	2·5317				2·5335	2·5353	44·89	8
4 1 0	2·5005	2·4984	45·59	2	2·5195	2·5172	45·23	2
$\bar{2}$ 3 2	2·4820	2·4830	45·89	10	2·4813	2·4829	45·89	10
0 3 2	2·4806				2·4821			
$\bar{4}$ 1 2	2·4675	2·4666	46·21	17	2·4734	2·4719	46·11	18
2 1 2	2·4635				2·4759			
3 3 0	2·4451	2·4448	46·65	3	2·4552	2·4547	46·45	3
$\bar{2}$ 1 3	2·4242	2·4170	47·22	1	2·4215	—		
$\bar{1}$ 1 3	2·4233				2·4221	—		

β angle for structures in Series 4 is now greater than the pseudoorthorhombic value of 109·73° does nevertheless suggest a distinct structural change.

4 Discussion

The present work shows that compositions in the series between dysprosium J-phase, $Dy_4Si_2O_7N_2$ and the structurally similar aluminate, $Dy_4Al_2O_9$, do not form a simple homogeneous solid solution. The end members index satisfactorily in space group $P2_1/a$ and have similar cuspidine-like structures, which extend as solid solutions in the ranges $0 \leq x \leq 0{\cdot}4$ and $1{\cdot}6 \leq x \leq 2{\cdot}0$. For most of the interval in between (i.e. $0{\cdot}5 \leq x \leq 1{\cdot}5$), a slightly different but nevertheless related structure is observed, characterised by its significantly reduced b axis repeat, and also by the increased intensities of odd 1 reflections barely visible in the other series. At the high-x end of this range ($1{\cdot}4 \leq x \leq 1{\cdot}5$), compounds show much simpler X-ray patterns which can be indexed on the basis of an orthorhombic cell. Finally, in the range $0{\cdot}8 \leq x \leq 1{\cdot}1$, one (or more) additional monoclinic J-phases occur with cell dimensions different from the Series 2 cell observed in this region.

Structural variants of cuspidine-based minerals are well known (e.g. Refs 23–25), and Merlino *et al.*[26] have summarised four different types of unit cell, based on different stackings of adjacent Si_2O_7 double tetrahedral units (Table 10). It is interesting that one sample of baghdadite[26] indexes on a pseudo-orthorhombic unit cell ($\alpha = 90{\cdot}04°$, $\beta = 90°$, $\gamma = 90°$) very similar to the Series 5 structures

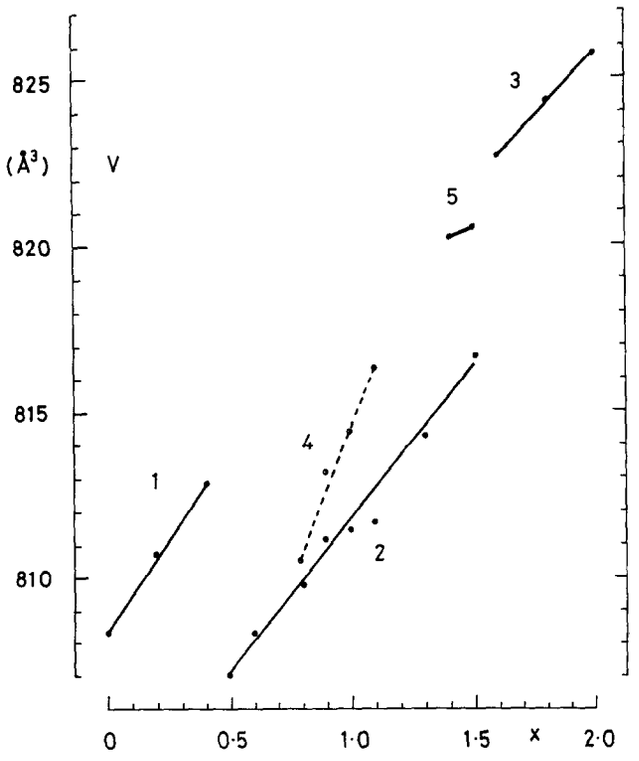

Fig. 7. Variation in unit cell volume with x, for $x = 0-2$ along the $Dy_4Si_{2-x}Al_xO_{7+x}N_{2-x}$ line.

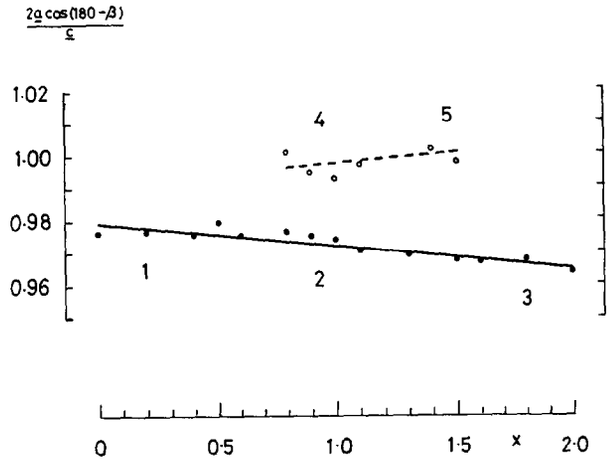

Fig. 8. Variation of $2a_m\cos(180-\beta)/c$ with x, for $x = 0-2$ along the $Dy_4Si_{2-x}Al_xO_{7+x}N_{2-x}$ line.

observed here. Further work is in progress to correlate the present structures with the structural variants discussed by Merlino *et al.*[26] More recently, there has been considerable interest in phase transformations in $(Ln,Y)_4Al_2O_9$ phases. Yamane *et al.*[27] observed a phase transformation in $Y_4Al_2O_9$ at 1377°C. Takizawa *et al.*[28] extended

Table 9. X-ray diffraction data for Dy J-phase Series 5 showing monoclinic and orthorhombic indexing at $x = 1{\cdot}4$

Monoclinic		*Orthorhombic*		$x = 1{\cdot}4$		
h k l	d_{calc}	*h k l*	d_{calc}	d_{obs}	$2\theta_{obs}$	I_{obs}
1 1 0	7·3971	1 1 0	7·3864	7·4078	15·02	43
0 2 0	5·2387	0 2 0	5·2436	5·2412	21·29	2
2 0 0	5·2225	2 0 0	5·2026	5·2236	21·36	8
1 2 0	4·6827	1 2 0	4·6826	—		
2 1 0	4·6740	2 1 0	4·6606	4·6754	23·90	48
2 2 0	3·6986	2 2 0	3·6932	3·6980	30·35	10
$\bar{1}$ 1 2	3·5286	0 1 2	3·5293	3·5270	31·86	8
$\bar{2}$ 0 2	3·5279	1 0 2	3·5262			
0 0 2	3·5269					
$\bar{2}$ 1 2	3·3434	1 1 2	3·3423	3·3424	33·67	13
0 1 2	3·3426					
1 3 0	3·3122	1 3 0	3·3137	—		
3 1 0	3·3040	3 1 0	3·2930	3·3018	34·10	46
$\bar{1}$ 2 2	3·0480	0 2 2	3·0491	3·0479	37·04	100
		2 0 2	3·0410			
$\bar{2}$ 2 2	2·9262	1 2 2	2·9261	—		
0 2 2	2·9257					
$\bar{3}$ 1 2	2·9243	2 1 2	2·9207	2·9234	38·67	62
1 1 2	2·9232					
2 3 0	2·9031	2 3 0	2·9016	2·8989	39·01	93
3 2 0	2·8997	3 2 0	2·8928			
$\bar{3}$ 2 2	2·6328	2 2 2	2·6306	2·6309	43·17	2
1 2 2	2·6320					
0 4 0	2·6194	0 4 0	2·6218	2·6191	43·38	31
4 0 0	2·6112	4 0 0	2·6013	—		
$\bar{1}$ 3 2	2·5550	0 3 2	2·5564	2·5604	44·43	3
$\bar{4}$ 0 2	2·5513	3 0 2	2·5456	2·5485	44·64	59
2 0 2	2·5502					
1 4 0	2·5407	1 4 0	2·5423	2·5404	44·79	16
4 1 0	2·5337	4 1 0	2·5248	2·5311	44·97	4
$\bar{2}$ 3 2	2·4820	1 3 2	2·4825	2·4799	45·95	29
0 3 2	2·4816					
$\bar{4}$ 1 2	2·4788	3 1 2	2·4738	2·4747	46·05	7
2 1 2	2·4778			2·4644	46·25	6
3 3 0	2·4657	3 3 0	2·4621			

Table 10. Different possible unit cells for mineral cuspidine-type compounds (after Ref. 26)

Type	*I*	*II*	*III*	*IV*
a (Å)	10·93	10·30	10·30	10·93
b (Å)	10·30	10·93	10·30	10·93
c (Å)	7·30	7·30	7·30	7·30
α (°)	90·0	109·5	90·0	109·5
β (°)	109·5	90·0	90·0	109·5
γ (°)	90·0	90·0	90·0	83·6

this work to mixed rare earth aluminates of the type $(Ho,La)_4Al_2O_9$ and $(Y,La)_4Al_2O_9$, which transformed to an orthorhombic form at high temperatures. The cell parameters for this orthorhombic compound were $a = 21{\cdot}093$, $b = 10{\cdot}554$, $c = 7{\cdot}499$ Å, but the indexed diffraction patterns showed only lines with h even and l even, indicative of a smaller sub-cell of dimensions $10{\cdot}546 \times 10{\cdot}554 \times 3{\cdot}750$ Å, similar to that observed for Series 5 compounds in the present work. Similar observations were made by Takizawa *et al.*[29] and by Shimada[30] for compositions in the $(Ln,La)_4Al_2O_9$ series, where Ln = Gd, Ho. More recently, Shimada *et al.*[31] have shown that for $Gd_4Al_2O_9$, the room temperature monoclinic form can transform at ~1100°C to a higher temperature monoclinic form, which in turn transforms to an orthorhombic modification at ~1400°C.

Since transformations occur in the pure oxide systems, it seems likely that they also occur in oxynitride systems. In the present work, varying the Si:Al and O:N ratios as the composition moves from $Dy_4Si_2O_7N_2$ to $Dy_4Al_2O_9$ slightly changes the geometry and the distribution of electrical charges in the structure, and this may well favour the stabilisation of the different structural modifications identified by Merlino *et al.* for mineral structures. Further work is in progress to characterise more fully the structures observed in these J-phase oxynitride systems.

5 Conclusions

Five slightly different types of cuspidine structure have been identified in the range of composition between the isostructural compounds $Dy_4Si_2O_7N_2$ and $Dy_4Al_2O_9$. Whereas the end members form solid solutions extending 20% of the way from either end, a structural change occurs at 25% $Dy_4Al_2O_9$, denoted by a marked decrease in the b-axis repeat, whilst at the 75% $Dy_4Al_2O_9$ 25% $Dy_4Si_2O_7N_2$ composition, the X-ray pattern markedly simplifies, with an apparently orthorhombic structure resulting. These phenomena are almost certainly related to the structural variants of the cuspidine structure observed in mineral systems, and also to the recently observed high temperature phase transformations observed in mixed rare earth $Ln_4Al_2O_9$ aluminates.

References

1. Saburi, S., Kawahara, A, Henmi, C., Kusachi, I. and Kihara, K., The refinement of the crystal structure of cuspidine. *Miner. J.*, 1977, **8**(5), 286–298.
2. Brandle, C. D. and Steinfink, H., The crystal structure of $Eu_4Al_2O_9$. *Inorg. Chem.*, 1969, **8**(6), 1320–1324.
3. Rae, A. W. J. M., Thompson, D. P., Pipkin, N. J. and Jack, K. H., The structure of yttrium silicon oxynitride and its role in the hot-pressing of silicon nitride with yttria additions. In *Special Ceramics* 6, ed. P. Popper. BCRA, Stoke on Trent, UK 1975, pp. 347–360.
4. Morgan, P. E. D., Comment on 'Reaction of Si_3N_4 with Al_2O_3 and Y_2O_3' and 'Silicon yttrium oxynitrides' by R. R. Wills.. *J. Am. Ceram. Soc.*, 1976, **59**(1–2), 86.
5. Lange, F. F., Singhal, S. C. and Kuznicki, R. C., Phase relations and stability studies in the Si_3N_4–SiO_2–Y_2O_3 pseudoternary system. *J. Am. Ceram. Soc.*, 1977, **60**(5–6), 249–252.
6. Marchand, R., Jayaweera, A., Verdier, P. and Lang, J., Preparation and characterisation of new oxynitrides in the Ln–Si–O–N system, melilites $Ln_2Si_3O_3N_4$ and cuspidines $Ln_4Si_2O_7N_2$. *C. R. Acad. Sci. Paris*, 1976, **C283**, 675–677.
7. MacKenzie, K. J. D., Gainsford, G. J. and Ryan, M. J., Rietveld refinement of the crystal structures of the yttrium silicon oxynitrides $Y_2Si_3O_3N_4$ (N-melilite) and $Y_4Si_2O_7N_2$ (J-phase). *Journal of the European Ceramic Society*, 1996, **16**, 553–560.
8. Rae, A. W. J. M. R., Yttrium silicon oxynitrides. Ph.D. thesis, University of Newcastle upon Tyne, 1976.
9. Thompson, D. P. Phase relationships in Y–Si–Al–O–N ceramics. In *Tailoring Multiphase and Composite Ceramics*, ed. R. E. Tressler, G. L. Messing, C. G. Pantano and R. E. Newnham. Plenum, New York. Materials Science Research vol. **20**, 1986, 79–92.
10. Sugyama, N., Ukyo, Y., Toshio, T. and Wada, S., Japanese Patent No. 05-279124, 1993.
11. Higuchi, Y., Okabe, M. and Kuroda, T., Japanese Patent No. 06-294013, 1994.
12. Yamashita, S., Tanaka, K. and Matsunosako, H., Japanese Patent No. 07-172927, 1995.
13. Nishimura, S., Japanese Patent No. 08-48565, 1996.
14. Coutures, J. P., Antic, E. and Caro, P., Obtention par trempe a partir de l'etat liquide d'une nouvelle phase dans le systeme $Nd_2O_3.Al_2O_3$. Etude comparative avec $Nd_4Ga_2O_9$. *Mats. Res. Bull.*, 1976, **11**, 699–706.
15. Mizuno, M., Yamada, T. and Noguchi, T., Phase diagram of the system Al_2O_3–Sm_2O_3 at high temperatures. *Yogyo-Kyokai-Shi*, 1977, **85**(8), 374–379.
16. Mizuno, M., Yamada, T. and Noguchi, T., Phase diagrams of the systems Al_2O_3–Eu_2O_3 and Al_2O_3–Gd_2O_3 at high temperatures. *Yogyo-Kyokai-Shi*, 1977, **85**(11), 544–548.
17. Mizuno, M., Yamada, T. and Noguchi, T., Phase diagrams of the system Al_2O_3–Dy_2O_3 at high temperatures.. *Yogyo-Kyokai-Shi*, 1978, **86**(8), 359–364.
18. Mizuno, M., Phase diagrams of the system Al_2O_3–Ho_2O_3 and Al_2O_3–Er_2O_3 at high temperatures. *Yogyo-Kyokai-Shi*, 1979, **87**(8), 405–412.
19. Mizuno, M. and Noguchi, T., Phase diagram of the system Al_2O_3–Yb_2O_3 at high temperatures. *Yogyo-Kyokai-Shi*, 1980, **88**(6), 240–242.
20. Nishimura, T. and Mitomo, M., Phase relationships in the system Si_3N_4–SiO_2–Yb_2O_3. *J. Mater. Res.*, 1995, **10**, 240–242.
21. Montorsi, M. and Appendino, P., Silicon terbium oxynitride of composition $Tb_4Si_2O_7N_2$. *Ceram. Bull.*, 1979, **58**(8), 789.

22. Wills, R. R., Stewart, R. W., Cunningham, J. A. and Wimmer, J. M., The silicon lanthanide oxynitrides. *J. Mater. Sci.*, 1976, **11**, 749–759.
23. Nickel, E. H., Rowland, J. F. and Maxwell, J. A., The composition and crystallography of niocalite. *Canadian Mineralogist*, 1958, **6**, 264–272.
24. Arden, H. M. and Gittins, J., Hiortdahlite from Kipawa River, Villedieu Township, Temiscaming County, Quebec, Canada. *Canadian Mineralogist*, 1974, **12**, 241–247.
25. Al-Hermezi, H. M., McKie, D. and Hall, A. J., Baghdadite, a new calcium zirconium silicate mineral from Iraq. *Min. Mag.*, 1986, **50**, 119–123.
26. Merlino, S. and Perchiazzi, N., Modular mineralogy in the cuspidine group of minerals. *Canadian Mineralogist*, 1988, **26**, 933–943.
27. Yamane, H., Omori, M, Okubo, A. and Hirai, T., High temperature phase transition of $Y_4Al_2O_9$. *J. Amer. Ceram. Soc.*, 1993, **76**(9), 2382–2384.
28. Takizawa, H, Shimada, M., Shimoyashiki, K. and Endo, T., Stress-induced phase transformation in the systems $(Ho_{1-x}La_x)_4Al_2O_9$ and $(Y_{1-x}La_x)_4Al_2O_9$. *J. Amer. Ceram. Soc.*, 1994, **77**, 2489–2490.
29. Takizawa, H., Kanou, S., Uchida, S., Shimada, M. and Endo, T., High temperature orthorhombic phase of $(R_{1-x}La_x)_4Al_2O_9$ (R = Gd, Ho). *J. Mat. Sci. Lett.*, 1996, **15**, 40–42.
30. Shimada, M., A stress-induced phase transformation of high temperature orthorhombic phase of $(R_{1-x}La_x)Al_2O_9$ (R = Gd, Ho). In *Engineering Ceramics '96*, NATO ASW ed. G. N. Babini and R. Metselaar. Kluwer, Dordrecht, The Netherlands)
31. Shimada, M. Yamane, H., Takizawa, H. and Endo, T., Phase transformation of $Gd_4Al_2O_9$ at high temperatures. In *Euro Ceramics V, Part 1, Key Engineering Materials* Vols 132–136, ed. D. Bortzmeyer, M. Boussuge, Th. Chartier, G. Fantozzi, G. Lozes and A. Rousset. Trans Tech, Zurich, Switzerland, 1997, pp. 647–650.